CHAPTER III

RESULTS AND DISCUSSION

3.1 Synthesis and Characterization of Cryptand-like Calix[4]arene Derivatives

Our research group has been interested in construction of calix[4]azacrowns as molecular receptors for many years. These calix[4]arenes possess both crown ether and nitrogen donor groups for binding metal ions. Moreover, some ammonium derivatives also exhibit good properties for binding anions by means of electrostatic and hydrogen bonding interaction.[80] All compounds were prepared from the lower rim modification of *p-tert*-butylcalix[4]arene with two bromoethoxy benzaldehydes, **1a** and **1b**, in the presence of K_2CO_3 as base.[81] Dialdehyde calix[4]arenes, **2a** and **2b**, were major products of this nucleophilic substitution reaction and served as important starting materials for other calix[4]azacrowns.[82] In contrast, trialdehyde derivatives, **3a** and **3b**, were obtained in very low yields (5% and 10%, respectively) and the synthetic process was therefore considered unsuitable.

As illustrated in chapter I, if considered carefully, it was clearly noticed that all of calixarenes that synthesized for transition metal ions complexation are 1,3-disubstituted or tetrasubstituted calix[4]arenes. Examples of trisubstituted compounds are really rare.[83] Nevertheless, this ligand type is a cage molecule (cryptand), which is able to encapsulate metal ions into its cavity, and has different binding ability as compared to the others. According to this idea, compounds **3a** and **3b**, were synthesized and utilized as key synthons in order to obtain new calix[4]cryptands.

In order to improve the yields of **3a** and **3b**, many bases, solvents systems and different reaction conditions were tried. In early attempts, we thought that stronger bases like NaH and $KOBu^t$ might probably give higher yields of **3a** and **3b** than K_2CO_3. Unfortunately, all reactions employing these two bases gave many undesired products, which are difficult to purify. The use of toluene and THF as solvents in the presence of aforementioned base was failed. This might be considered that *p-tert*-butylcalix[4]arene was not dissolve in THF even it formed anionic species in the treatment of base. Non-polar solvent like toluene also did not stabilize anionic species even if the starting compound was completely dissolved when heating at reflux.

According to the literature review, the trisubstituted calix[4]arenes can be obtained from the reactions of calix[4]arenes with alkylating agents in the presence of BaO or $Ba(OH)_2$ in DMF.[32, 84, 85] At first, using BaO in DMF at reflux condition was failed. However, when the temperature was reduced to about 70 °C, two desired products **3a** and **3b** were observed in the TLC plate. The reason could be ascribed to the fact that DMF was decomposed at reflux temperature leading to the formation of CO and dimethylamine. Both compounds might uncontrollably reacted with bromoethoxybenzaldehyde and led to many by-products, which observed in the reaction.

Therefore, compound **3b** was synthesized by the reaction between *p-tert*-butylcalix[4]arene and **1b** in the presence of BaO as base and DMF as solvent for 7 days. The reaction temperature was kept under 70 °C to avoid the decomposition of the solvent. Both dialdehyde and trialdehyde calix[4]arenes, **2b** and **3b** were obtained and purified by silica gel column chromatography using dichloromethane and the mixture of dichloromethane and ethyl acetate (98:2) as eluents. The yields of compounds **2b** and **3b** were 2% and 46%, respectively. Higher yield of **3b** as compared to **3a** may stem from the less steric hindrance of substituents on calix[4] arene framework in **3b**. Calix[4]arene **2b** showed a singlet signal of C**H**=O at 10.06 ppm in ^{1}H-NMR spectrum. In addition, this derivative existed in cone conformation as evidenced by the presence of ArCH_2Ar as two doublets at 4.54 and 3.49 ppm with coupling constant (J) = 13.3 Hz as well as *tert*-butyl proton signals which appeared at 1.47 (the substituted phenol rings) and 1.17 ppm (the unsubstituted rings). ^{13}C-NMR

spectrum of **2b** exhibited only one type of methylene bridge carbon.[86] MALDI-TOF mass spectra also supported the proposed structure of this derivative showing an intense line at m/z 945.0.

In contrast of **2b**, ^{1}H-NMR spectrum of compounds **3b** exhibited two signals of C**H**=O at 9.76 and 9.64 ppm in 1:2 integral ratio. The four groups of doublet signals at 4.47, 4.46, 3.33 and 3.27 ppm with different *J*-coupling constants indicated that the methylene bridge protons were unsymmetrical and this calix[4]arene existed in the pinched-cone conformation. Its ^{13}C-NMR spectrum has three different signals of **C**($\mathbf{C}H_3$)$_3$ that was implied that the *tert*-butyl groups were not identical. MALDI-TOF MS showed an intense peak at m/z 1093.6 due to the [M + 1] and elemental analysis was in good agreement with the proposed structure.

The condensation reaction of **3b** with 1.1 equivalents of *tris*(2-aminoethyl) amine in a mixture of methanol and acetonitrile employing a high dilution technique yielded a creamy white precipitate of calix[4]arene imine **4b** (97%). The characteristic signals of C**H**=O disappeared, however, the RN=C**H** proton signals appeared at 7.92 and 8.08 ppm with 1:2 integral ratio in ^{1}H-NMR spectrum of **4b**. Similar to its trialdehyde analogue, this imine calix[4]arene conformation was pinched-cone which can be deduced from the existence of Ar$\mathbf{C}H_2$Ar AB system signals at 4.93 and 3.34 ($J_{H\text{-}H}$ = 13.3 Hz) ppm and at 4.34 and 3.24 ($J_{H\text{-}H}$ = 12.5 Hz) ppm. Furthermore, C($\mathbf{C}H_3$)$_3$ protons showed three singlet lines at 1.40, 1.37 and 0.85 ppm in 1:1:2 ratio, respectively supported that **4b** was more rigid than **3b** when the the **tren** moiety was introduced into the molecule. MALDI -TOF mass spectrum of **4b** had a strongest peak at 1185.7 m/z and its ^{13}C-NMR spectrum showed two different imine carbon atoms at 161.46 and 165.42 ppm as well as methylene bridge carbons at 30.47 and 30.69 ppm.

Reduction of **4b** to **5b** was carried out by addition of 24 equivalents of sodium borohydride into the solution of **4b** in CH_2Cl_2 and subsequently acidified with dilute HCl/CH_3OH (0.74% v/v), affording an ammonium salt calix[4]arene derivative **5b** in almost 84% yield. This compound exhibited very broad signals in the ^{1}H-NMR spectrum due to the positive charge of the ammonium cations. The positive charge groups, Ar$CH_2N\mathbf{H}_2^+$ appeared at 8.64 and 8.24 ppm with an integral ratio of 2:1.

^{1}H-NMR spectrum of **5b** also exhibited four doublet signals due to Ar**C**$\mathbf{H}_2$Ar at 4.55, 4.45, 3.29 and 3.24 ppm indicating that the molecule is in the pinched-cone conformation. MALDI-TOF MS showed an intense signal at m/z 1191.8 corresponding to the mass of **5b** with the four hydrogen chloride molecules stripped off. However, elemental analysis results supported the existence of this ammonium derivative.

Finally, the ammonium salt calix[4]arene **5b** was converted to tetraamine calix [4]arene **6b**. The 4 equivalents of NaOH dissolved in methanol were added into the solution of **5b** in dichloromethane. After extracted with water and dichloromethane, compounds **6b** was obtained as white needle-like crystal (74%) after slowly recrystallized from a mixture of CH_2Cl_2 and CH_3OH. Almost all proton signals in ^{1}H-NMR spectrum shifted upfield due to the high electron density of amine groups. The chemical shift at 8.64 and 8.24 disappeared and aromatic protons of calix[4]arene unit existed at about 7.11 and 6.60 ppm. In addition, ^{1}H-NMR spectrum of **6b** exhibited four doublet signals due to Ar**C**$\mathbf{H}_2$Ar at 4.78, 4.40, 3.27 and 3.26 ppm indicating that the molecule is in the pinched-cone conformation as same as its ammonium derivative **5b**. MALDI-TOF mass spectrum showed an intense peak at m/z 1191.2 that corresponding to the mass of **6b** and elemental analysis also supported the proposed structure of **6b**.

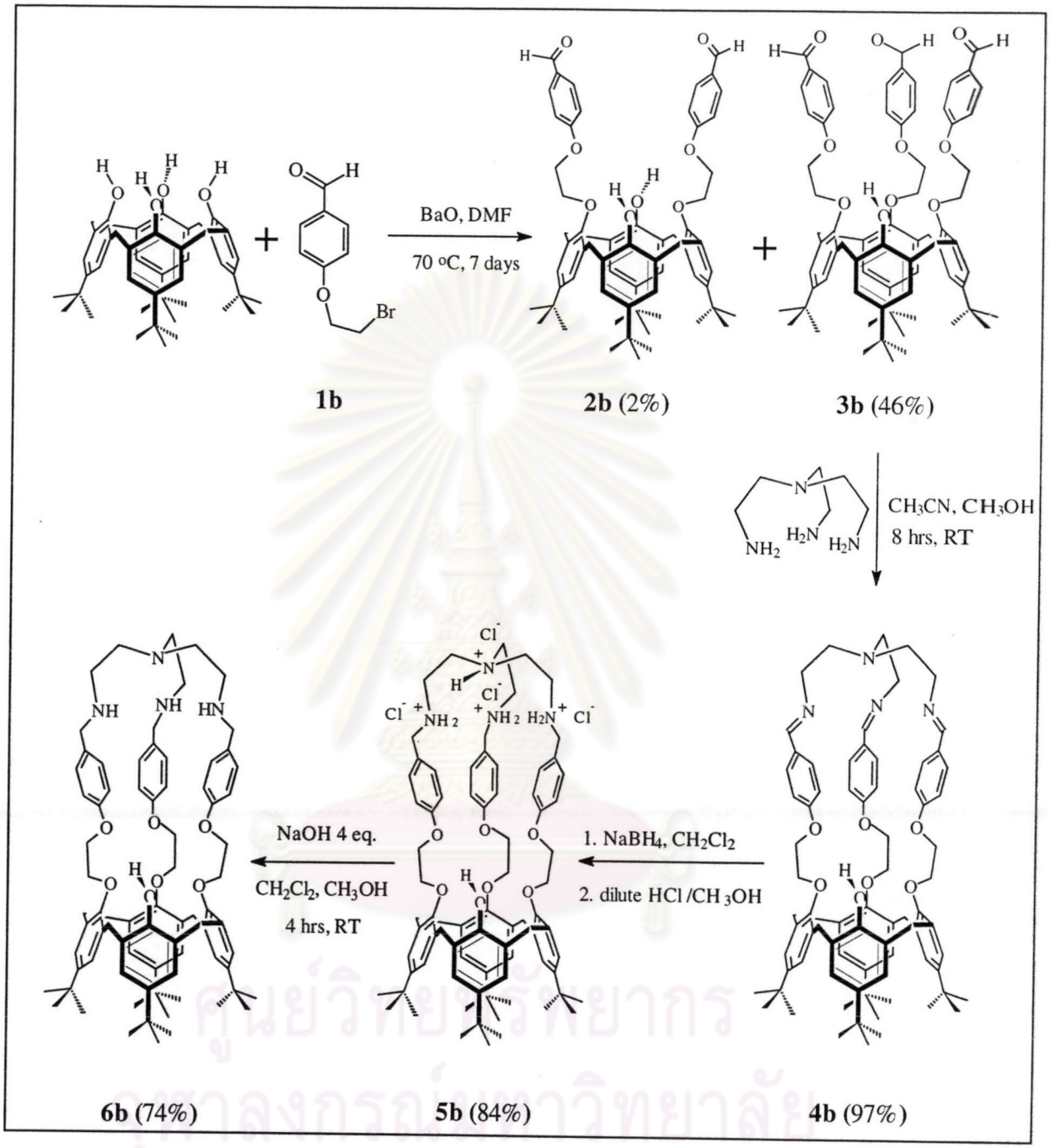

Scheme 3.1 Synthetic pathway of calix[4]cryptand **6b**.

3.2 Basicity and Metal Ions Complexation Studies

Ligands **6a** and **6b** contain four nitrogen donor atoms, which can encapsulate metal ions into their cavities. Both of them were used to study their binding ability towards three divalent transition metal ions: Co^{2+}, Cu^{2+} and Zn^{2+}. Compounds **6a** and **6b** have different cavity sizes that can affect to the stability of the complexes.

Potentiometric titration was employed to investigate the basicity and complexation abilities of **6a** and **6b**. At least 45 data points from each titration were used for computer refinement in order to obtain protonation constants and stability constants for metal complexes, which were evaluated by the program SUPERQUAD.

3.2.1 Protonation Constants of Ligands 6a and 6b

25,26,27-*N*, *N'*, *N''*-tris((2-ethoxy)benzyl)ethylenetetraamine-*p-tert*-butylcalix [4]arene.4HCl , **5a**, and 25,26,27-*N*, *N'*, *N''*-tris((4-ethoxy)benzyl)ethylenetetraamine -*p-tert*-butylcalix[4]arene.4HCl , **5b**, were employed for determination of the protonation constants. The advantage of employment of calix[4]arenes **5a** and **5b** instead of **6a** and **6b** is that the methanolic solutions of **5a** and **5b** do not undergo side reactions which affects the concentration of the ligands in solutions, while undesired reactions are possibly occurred in case of using **6a** and **6b** directly.Nonetheless, the titration results are related to the proton affinity of two neutral calix[4]arenes 25,26,27-*N*, *N'*, *N''*-tris((2-ethoxy)benzyl)ethylenetetraamine-*p-tert*-butylcalix[4] arene, **6a**, and 25,26,27-*N*, *N'*, *N''*-tris((4-ethoxy)benzyl)ethylenetetra amine-*p-tert*-butylcalix[4]arene, **6b** since the deprotonation of **5a** and **5b** occurred during the titration experiments to give **6a** and **6b**, respectively.

The experimental titration curve of **6a** and **6b** in 0.01 M $Bu_4NCF_3SO_3$ in methanol at different initial concentrations of ligand and proton are shown in Figures 3.1 and 3.2, respectively. The X-axis is the equivalent, which defined as follows:

$$\text{Equivalent} = \frac{n_{OH} - n_{H^+}}{n_{ligand}} \qquad (2)$$

Where $\mathbf{n_{OH^-}}$ is the mole of OH^- at each titration point, $\mathbf{n_{H^+}}$ is the total mole of H^+ in the solution for each experiment and $\mathbf{n_{ligand}}$ equals to the total mole of a ligand in the experimental solution. According to Figures 3.1 and 3.2, each equivalent point on titration curves does not exhibit the ideal characteristic of theoretical S-shape titration curve. The first three deprotonation steps are observed clearly while the fourth step are scarcely detected in the experimental titration curve for **6a**. However, titration curves of ligand **6b** show 4 distinguishable deprotonation steps that reveal the available four protons on the ligand.

The plots between $\bar{p}$ (the protonation formation function), equation (**3**), and log $[H^+]$ for ligands **6a** and **6b** in 0.01 M $Bu_4NCF_3SO_3$ in methanol are also shown in Figures 3.3 and 3.4, respectively. The value of $\bar{p}$ is defined as the average number of proton **H** bound to the ligand **L**:

$$\bar{p} = \frac{[H^+]_T - [H^+] - [OH^-]}{[L]_T} \qquad (3)$$

When $[H^+]$ is concentration of the free proton obtained from the measurement. $[OH^-]$ is the concentration due to the titrant that converted to $[H^+]$ by the relation of the autoprotolysis constant of methanol ($\log K_{meOH} = -16.7$).

Considering the relationship between $\bar{p}$ and log $[H^+]$ displayed in Figures 3.3 and 3.4, it indicates that four protons are possibly accommodated in the molecules of **6a** and **6b**. For compound **6a**, the average number of proton bound is about 2 in the range of log $[H^+]$ from –8.6 to –6.0. The third proton attachment is completed at concentration of proton about 2.08×10^{-6} M. The $\bar{p}$ value of **6a** reaches 4 at the log $[H^+]$ higher than -3.0. Therefore, this result is agreed with the structure of **6a**, which contains four nitrogen atoms and can receive four protons in its molecule. Ligand **6b** has a similar relationship between $\bar{p}$ and log $[H^+]$ like that happened in **6a**. However, there is something quite different. The number of attached proton is 2 at around the range of log $[H^+]$ from -8.6 to –6.6 for **6b** (Figure 3.4). After that, the third proton is occupied at log $[H^+]$ = -6.3. The $\bar{p}$ value rapidly increases to 4 when the concentration of H^+ in the solution nearly reaches 3.95×10^{-4} M.

This implies that **6b** is slightly easier to form LH_4^{4+} species than its *ortho* derivative.

The values of protonation constants were calculated by SUPERQUAD program with the chi-square value less than 12.60 in order to reach 95% confidence. The protonation constants of **6a** and **6b** in 1.00 x 10^{-2} M $Bu_4NCF_3SO_3$ in methanol at 25 °C are shown in Table 3.1.

Table 3.1 Logarithm of the protonation constants of calix[4]arenes **6a** and **6b** in 1.00 x 10^{-2} M $Bu_4NCF_3SO_3$ at 25 °C.

Equilibrium	log K	
	Ligand **6a**	Ligand **6b**
K_1: $L + H^+ \rightleftharpoons LH^+$	12.03 ± 0.01	10.79 ± 0.04
K_2: $LH^+ + H^+ \rightleftharpoons LH_2^{2+}$	10.17 ± 0.01	9.35 ± 0.04
K_3: $LH_2^{2+} + H^+ \rightleftharpoons LH_3^{3+}$	6.95 ± 0.02	7.46 ± 0.04
K_4: $LH_3^{3+} + H^+ \rightleftharpoons LH_4^{4+}$	4.44 ± 0.03	5.33 ± 0.04

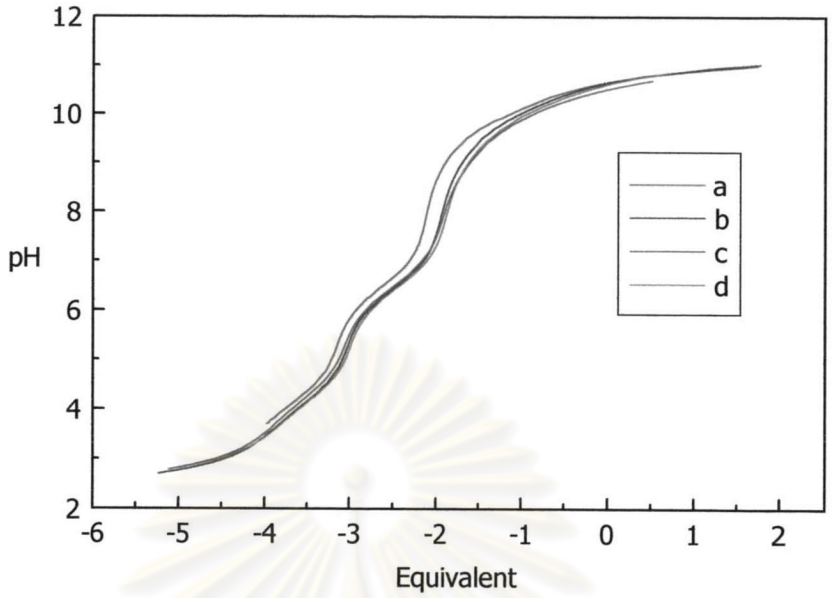

Figure 3.1 Potentiometric titration curves of **6a** in 1.00 x 10^{-2} M $Bu_4NCF_3SO_3$ in methanol at various ratio of **6a** : proton: (a) 1.014 mM : 4.056 mM, (b) 0.922 mM : 8.912 mM, (c) 0.845 mM : 8.912 mM and (d) 0.922 mM : 8.912 mM.

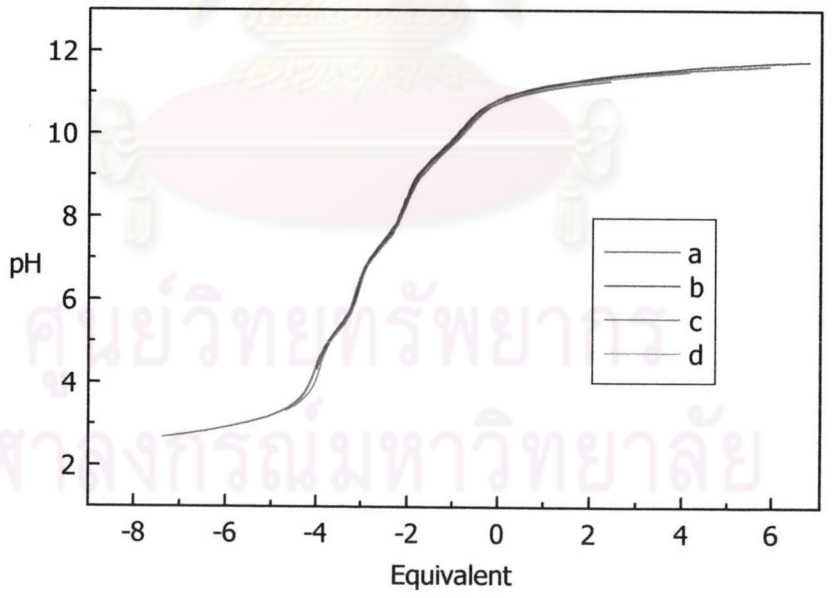

Figure 3.2 Potentiometric titration curves of **6b** in 1.00 x 10^{-2} M $Bu_4NCF_3SO_3$ in methanol at various ratio of **6b** : proton: (a) 1.007 mM : 4.028 mM, (b) 1.007 mM : 4.028 mM, (c) 0.839 mM : 11.557 mM and (d) 0.915 mM : 8.134 mM.

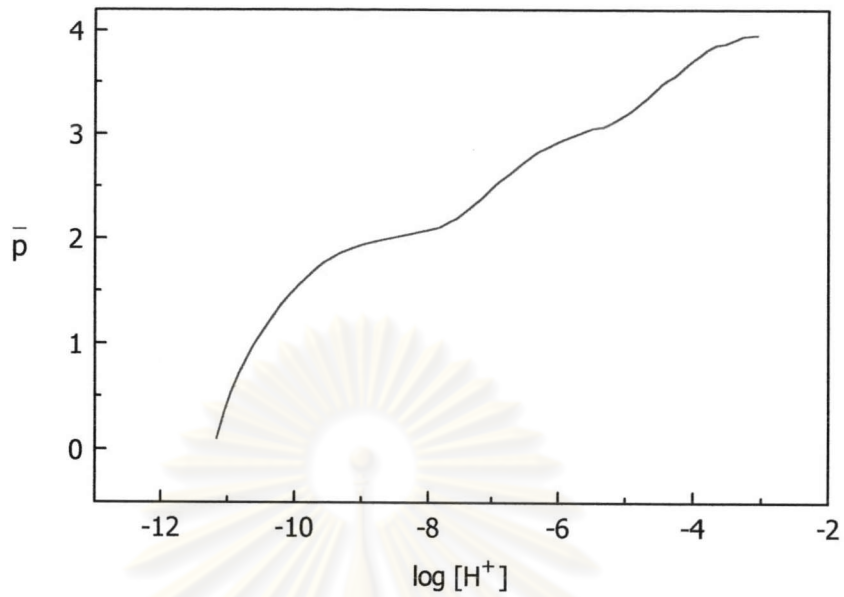

Figure 3.3 Plot between $\bar{p}$ and log [H^+] for **6a** in 1.00 x 10^{-2} M $Bu_4NCF_3SO_3$ in methanol at ratio of **6a** : proton = 0.922 mM : 8.912 mM.

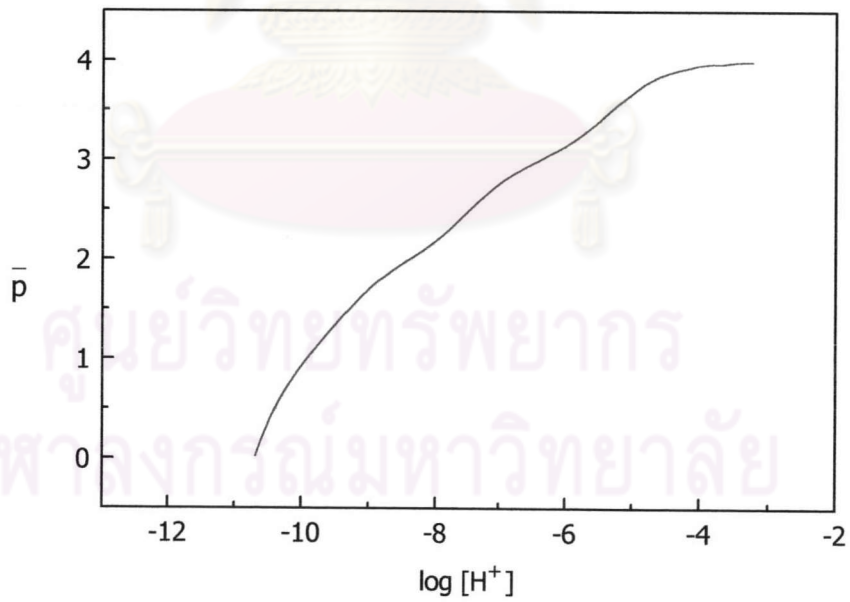

Figure 3.4 Plot between $\bar{p}$ and log [H^+] for **6b** in 1.00 x 10^{-2} M $Bu_4NCF_3SO_3$ in methanol at ratio of **6b** : proton = 0.915 mM : 8.134 mM.

According to the results shown in Table 3.1, both compounds **6a** and **6b** can bind up to four protons in the pH range 2-12 and show high basicity in the first two protonation steps, with the first constants log K_1 = 12.02 and 10.79 for **6a** and **6b**, respectively. The high K_1 value can be explained that the first proton has many alternate sites to add on the ones of three secondary amine's nitrogen atom in the **tren** moiety. However, it is obvious that the first protonation constant of **6a** is higher than that of **6b**. This outcome may stem from the fact that compound **6a** has nitrogen substituents at *ortho* position in which the neighboring nitrogen atoms can form intramolecular hydrogen bonding better than *para*-position in compound **6b**. This result leads to the more partial negative charge on nitrogen atoms and more positive charge at hydrogen atoms in **6a**. Therefore, the nitrogen donors in **6a** have higher electron density and higher proton affinity than those of **6b** leading to the better electron donation.

Ligand **6a** shows similar basicity constants in the second protonation step with log K_2 = 10.13, while the values dramatically decrease in the third proton received step (log K_3 = 6.95) and the fourth protonation constant (log K_4 = 4.44). The big gap of 3.18 logarithmic unit is detected between the second and third protonation constants. Considering the number of the protonated sites and their locations, this the trend in the constant values can be rationalized in terms of minimization of the electrostatic repulsion between positive charges in the protonated species. In other words, the first two protons can occupy alternate positions in the ligand separated by other unprotonated sites; the lower affinity of **6a** towards the third and fourth protonation is probably due to the unfavorable electrostatic repulsion from the neighboring ammonium groups.

Compound **6b** exhibits slightly lower protonation ability for the second proton addition (log K_2 = 9.35) than its *ortho* analogue. However, for the third and fourth protonation, ligand **6b** shows higher basicity constants than **6a** (log K_3 = 7.46 and log K_4 = 5.33) and the gap between the supplement of second and third proton is only about 1.89 logarithm unit. These results can be rationalized in term of the minimization of electrostatic repulsion. Although both calix[4]arenes have a similar protonation the trend in the same pH range, **6b** is less steric and each binding

site is more separated apart from each other. Thus, the third and fourth proton bindings of calix[4]arene **6b** are not so difficult to take place and the undesired positive charge repulsion is minimized inducing to great proton affinity of the other nitrogen atoms of the **tren** unit.

The species distribution plot of **6a** in 1.00 x 10^{-2} M $Bu_4NCF_3SO_3$ in methanol at 25°C (Figure 3.5) shows all four protonated species in the pH range between 3 – 11.5. The $\mathbf{LH_4^{4+}}$ is found in the acidic range of the solution. The population of this species is dramatically decreased from 96% at pH 3.0 to less than 1% at pH higher than 6.3. The three protonated species exists at the pH range of 3.2 to 8.5. The predominant species of **6a** in the solution is the $\mathbf{LH_2^{2+}}$ which has a maximum percentage at pH = 8.5 (94%) and appears at the pH range from 5.3 to 11.3. The $\mathbf{LH^+}$ population does not reach higher than 80% at pH 10.9. At the pH values more than 10.8, the free **L** species is tendiously increased while the LH^+ concentration is slowly decreased. Unfortunately, the experimental data at pH higher than 11.5 cannot be obtained. So, the maximum percentage of free **L** species cannot be exactly estimated.

In Figure 3.6, the species distribution plot of **6b** in 1.00 x 10^{-2} M $Bu_4NCF_3SO_3$ in methanol at 25 °C, exhibits the slightly different characteristic when compared with its *ortho* isomer. For **6b**, the population of $\mathbf{LH_4^{4+}}$ is decreased from 99% at pH = 3.3 to less than 5% at pH = 6.6. The $\mathbf{LH_3^{3+}}$ appears at the pH range of 3.9 to 8.6 and its concentration reached maximum at pH = 6.4 (85%). At pH higher than 7.3, the main species in the solution is $\mathbf{LH_2^{2+}}$. Unlike **6a**, this species is not a dominant species in the experimental range. The ratio of $\mathbf{LH^+}$: $\mathbf{LH_2^{2+}}$ is 50:50 at pH = 9.31 while the same ratio is observed at 10.7 in case of **6a**. This result can be explained in the term of the stability of the protonated species of both ligands. The $\mathbf{LH_2^{2+}}$ species of **6a** has the equilibrium constant higher than **6b** (see Table 3.1) and therefore it is more difficult to change from stable diprotonated to monoprotonated species. In case of $\mathbf{LH^+}$, its population is highest at 9.94 (72%) and gradually decreased to less than 20% at pH = 11.3. Free ligand **L** of **6b** is first detected at pH = 9.6 (less than 10%) and its concentration is accumulated until it reached 84% at pH = 11.5.

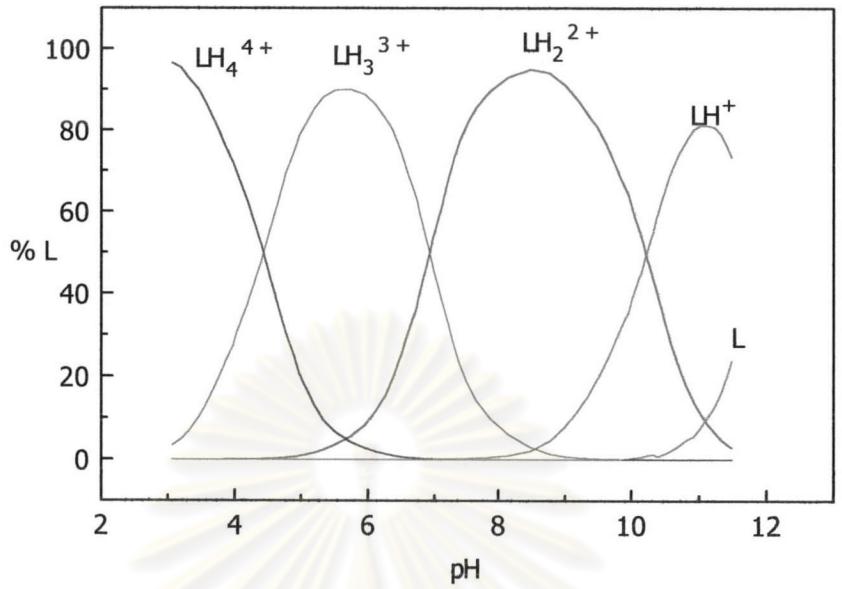

Figure 3.5 Species distribution plot of **6a** in 1.00 x 10^{-2} M $Bu_4NCF_3SO_3$ in methanol at 25 °C, C_L = 0.922 mM.

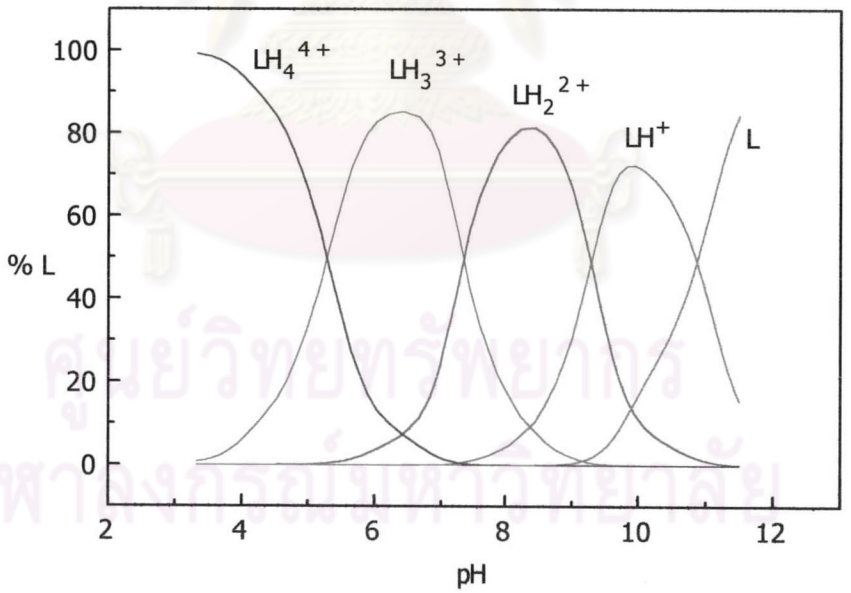

Figure 3.6 Species distribution plot of **6b** in 1.00 x 10^{-2} M $Bu_4NCF_3SO_3$ in methanol at 25 °C, C_L = 0.915 mM.

The basicity behaviour of **6a** and **6b** are quite similar to that of the other related cryptands such as R3Bm, R3Bp and RGT (Figure 3.7), which their proton affinities were studied in 0.1 M Et_4NClO_4 in water at 25 °C by means of potentiometric titration. The protonation constants of R3Bm, R3Bp and RGT are presented in Table 3.2.

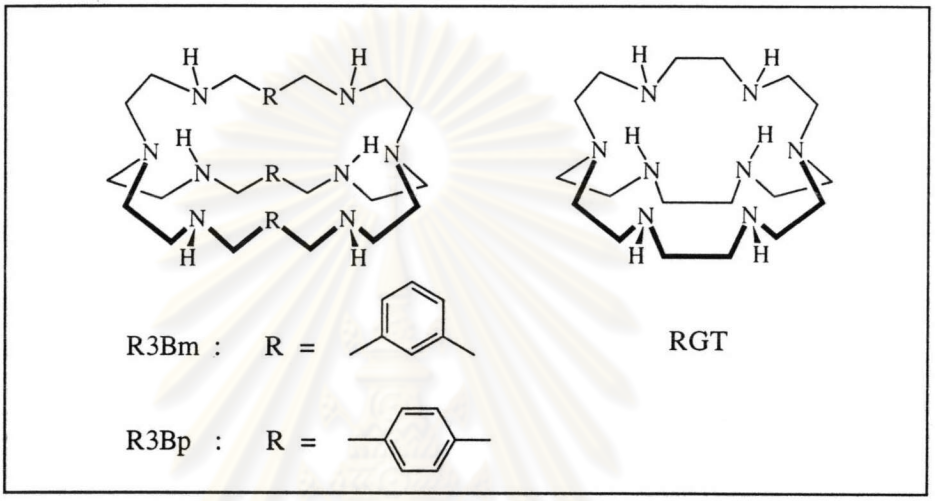

Figure 3.7 Structures of polyazacryptands R3Bm, R3Bp and RGT

Table 3.2 Logarithm of the protonation constants of R3Bm, R3Bp and RGT in 0.1 M Et_4NClO_4 in water at 25°C.[87]

log K_i (i = 1-6)	R3Bm	R3Bp	RGT
log K_1	9.8 ± 0.3	9.6 ± 0.1	10.6 ± 0.1
log K_2	9.17 ± 0.06	9.00 ± 0.04	9.62 ± 0.06
log K_3	8.5 ± 0.2	8.62 ± 0.08	7.91 ± 0.05
log K_4	7.21 ± 0.04	7.4 ± 0.1	5.65 ± 0.05
log K_5	6.9 ± 0.1	6.7 ± 0.1	-
log K_6	6.70 ± 0.05	6.52 ± 0.3	-

Considering the protonation constants of three azacryptands as shown in Table 3.2, cryptand R3Bm and R3Bp exhibit six protonation constants while RGT has only four. The trend of protonation constant of RGT is quite comparable to **6a** and **6b** than other azacryptands. Although structures of R3Bm and R3Bp are similar to **6a** and **6b**, both of them have eight nitrogen atoms while our ligands containing only four. However, R3Bm and R3Bp have only six protonation constants instead of possible eight. Only secondary amines on R3Bm and R3Bp are accessible to protonate. The remaining tertiary amines at the edge of the **tren** units are possibly not involved in the proton affinity of R3Bm and R3Bp. The major reason of this phenomenon can be rationalized in term of the distance between each nitrogen atoms. The position of donor atoms in R3Bm and R3Bp may be too close together. When the last secondary amine group is occupied by proton, the electronic repulsion of positive charges is too much and the further protonation at tertiary amine atom is totally prohibited. For cryptand RGT, the ethylene bridge that linked between secondary amine positions may not be large enough to split the nitrogen atoms into the appropriate position that the total positive charged repulsion is minimum. Therefore, only four protonation reactions are observed.

On the other hand, the tertiary amine group in ligands **6a** and **6b** is available for protonation. Commonly, the gas-phase and the solution acid-base properties of alkylamines are quite different. In gas phase, the basic strength of alkylamines increases with the increasing number of alkyl substituents at the nitrogen atom, which can be considered in terms of inductive and polarization effects. However, in the protic solutions, amines are solvated by solvent molecules and this leading to the increasing of the base strength of all amines containing free hydrogen atoms. The main reason is the positively charged ammonium ions that possess more acidic hydrogen will be better solvated than ones which have less protons.[88] We suggest that the introduction of the **tren** unit into calix[4]arene framework may affects to the space between nitrogen binding sites. All donor atoms are separated from one another to the suitable position, which the electronic repulsion is minimized and suitable for the fourth protonation reaction at tertiary amine group of the **tren** moiety. The presence of the calix[4]arene unit may thus enhance the possibility of the protonation at low proton affinity atoms such as tertiary amine in the solution.

3.2.2 Complexation Properties of Ligands 6a and 6b towards Co^{2+}, Cu^{2+} and Zn^{2+} ions

Compounds **6a** and **6b** possess four nitrogen donor atoms at the binding sites. Therefore, they are expected to bind first-row divalent transition metal ions such as Co^{2+}, Cu^{2+} and Zn^{2+} to give high stable complexes. Nevertheless, ligand **6a** has different size of the binding cavity in comparison with **6b**. So, we aim to investigate the effects of the size of the binding cavity and flexibility of the ligand that controlled the stability of the complex.

The binding ability studies of **6a** and **6b** towards Co^{2+}, Cu^{2+} and Zn^{2+} were carried out by means of potentiometric titration using a competitive method with the proton. The concentration of each species is measured versus pH that changed during experiments by addition of base. The pH values in titration curves are perturbed in the presence of metal ions leading to a significant pH drop when compared to the titration curves of the calix[4]arenes alone.

The titration curves of the complexes between ligand **6a** and **6b** with Cu^{2+}, Zn^{2+} and Co^{2+} ions in 1.00 x 10^{-2} M $Bu_4NCF_3SO_3$ in methanol are illustrated in Figures 3.8, 3.9 and 3.10, respectively.

The other valuable secondary concentration variable that obtained from the evaluation of stability constants is 'the complex formation function' ($\bar{n}$), which defined as the average number of ligand, L, attached to the metal, M. This parameter can be written as follows:

$$\bar{n} = \frac{[L]_T - [L]}{[M]_T} = \frac{\text{total bound ligand}}{\text{total metal}} \qquad (4)$$

The plot between the complex formation function ($\bar{n}$) and the logarithm of concentration of ligand L (log [L]) will give the information about the types of the complex formed similar to the plot between $\bar{p}$ and log [H^+] indicated about the totally proton affinity of the ligands.

The plot between $\bar{n}$ versus the log [L] of calix[4]arenes **6a** and **6b** with Cu^{2+}, Zn^{2+} and Co^{2+} ions in 1.00 x 10^{-2} M $Bu_4NCF_3SO_3$ in methanol are shown in Figures 3.9, 3.10 and 3.11, respectively.

According to Figures 3.11, 3.12 and 3.13, the results show that ligands **6a** and **6b** form only mononuclear complex (ML^{2+}) with Cu^{2+} due to the plots of $\bar{n}$ versus log [L] reach 1.0 at log [L] = -14.29 and –14.03, respectively. The 1:1 complexes are observed in the presence of Co^{2+}, which the $\bar{n}$ values reach 1.0 at log [L] = -5.42 for **6a** and log [L] = -5.92 in case of **6b**. However, the zinc complexes of **6a** and **6b** exhibit significant difference in term of complex formation. The $\bar{n}$ values increase slowly as the function of log [L] and reach 0.5 when the log [L] of ligand **6a** and **6b** are –9.99 and –8.49, respectively. When the concentrations of ligands exceed 5.19 x 10^{-7} M (for **6a**) and 1.48 x 10^{-4} M (for **6b**), the final maximum $\bar{n}$ values are 1.0. These may indicate that zinc binuclear complexes exist in the low concentration of ligands while mononuclear complexes will be detected at high concentration of free ligands. In addition, It also implies that zinc binuclear complexes are the most stable species in the medium pH range and mononuclear complexes are predominant species in the alkaline solution.

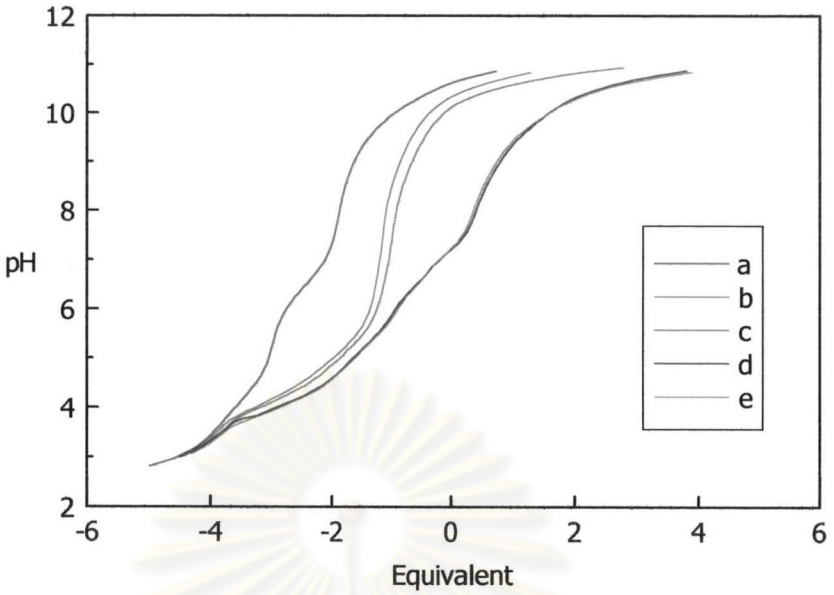

A

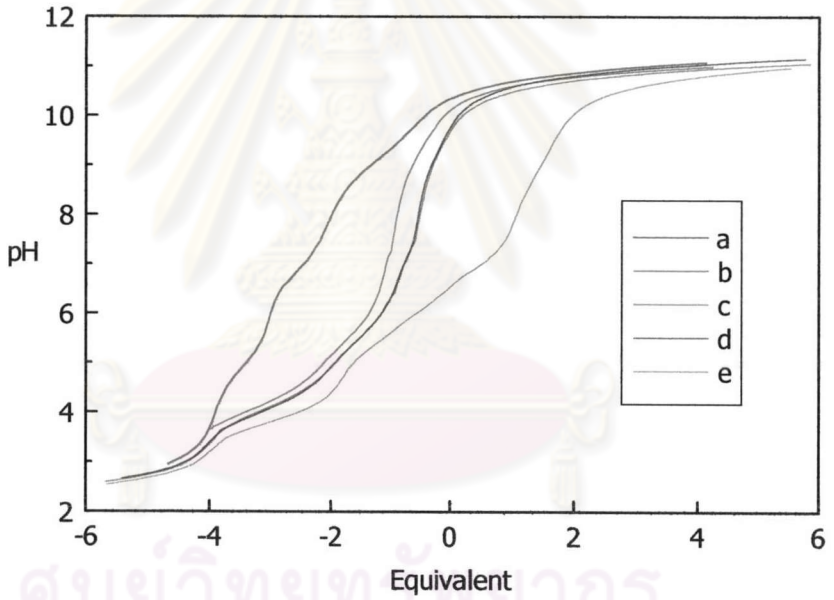

B

Figure 3.8 Potentiometric titration curves of

A) ligand **6a** with Cu^{2+} ion at various ratio of **6a** : Cu^{2+} : (a) 0.922 mM : 0 mM, (b) 0.882 mM : 0.833 mM, (c) 0.845 mM : 0.846 mM, (d) 0.811 mM : 1.625 mM and (e) 0.780 mM : 1.562 mM.

B) ligand **6b** with Cu^{2+} ion at various ratio of **6b** : Cu^{2+} : (a) 0.915 mM : 0 mM, (b) 0.922 mM : 0.923 mM, (c) 0.845 mM : 0.846 mM, (d) 0.845 mM : 0.846 mM and (e) 0.780 mM : 1.562 mM.

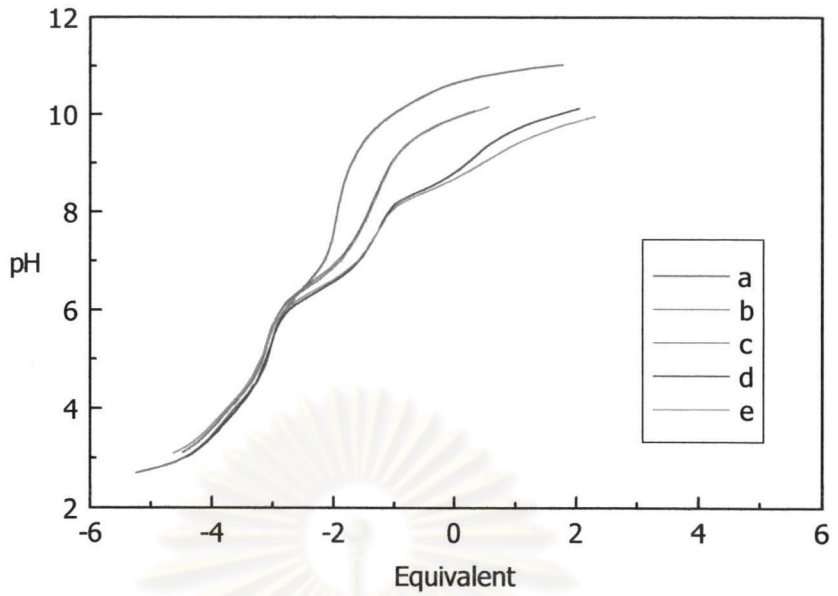

A

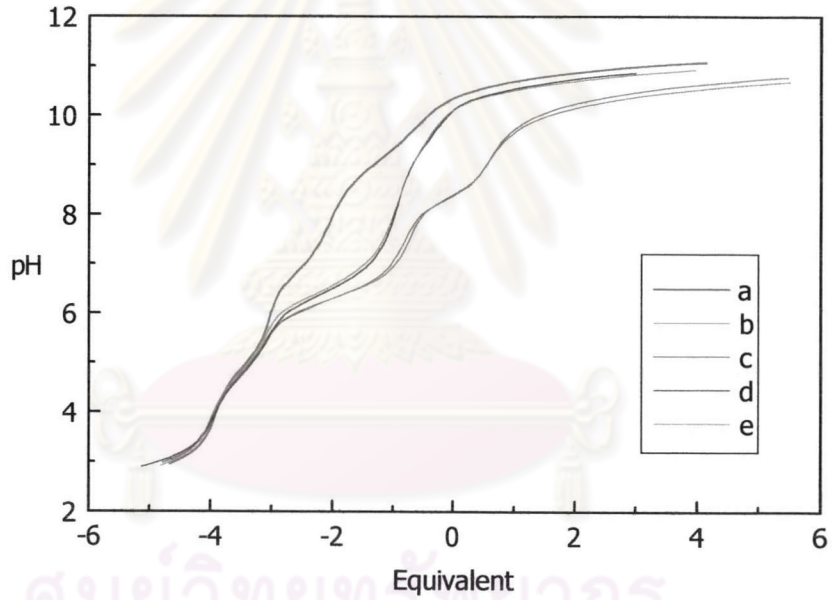

B

Figure 3.9 Potentiometric titration curves of

A) ligand **6a** with Zn^{2+} ion at various ratio of **6a** : Zn^{2+} : (a) 0.922 mM : 0 mM, (b) 0.875 mM : 0.885 mM, (c) 0.839 mM : 0.845 mM, (d) 0.805 mM : 1.629 mM and (e) 0.774 mM : 1.566 mM.

B) ligand **6b** with Zn^{2+} ion at various ratio of **6b** : Zn^{2+} : (a) 0.915 mM : 0 mM, (b) 0.840 mM : 0.835 mM, (c) 0.876 mM : 0.871 mM, (d) 0.806 mM : 1.629 mM and (e) 0.775 mM : 1.566 mM.

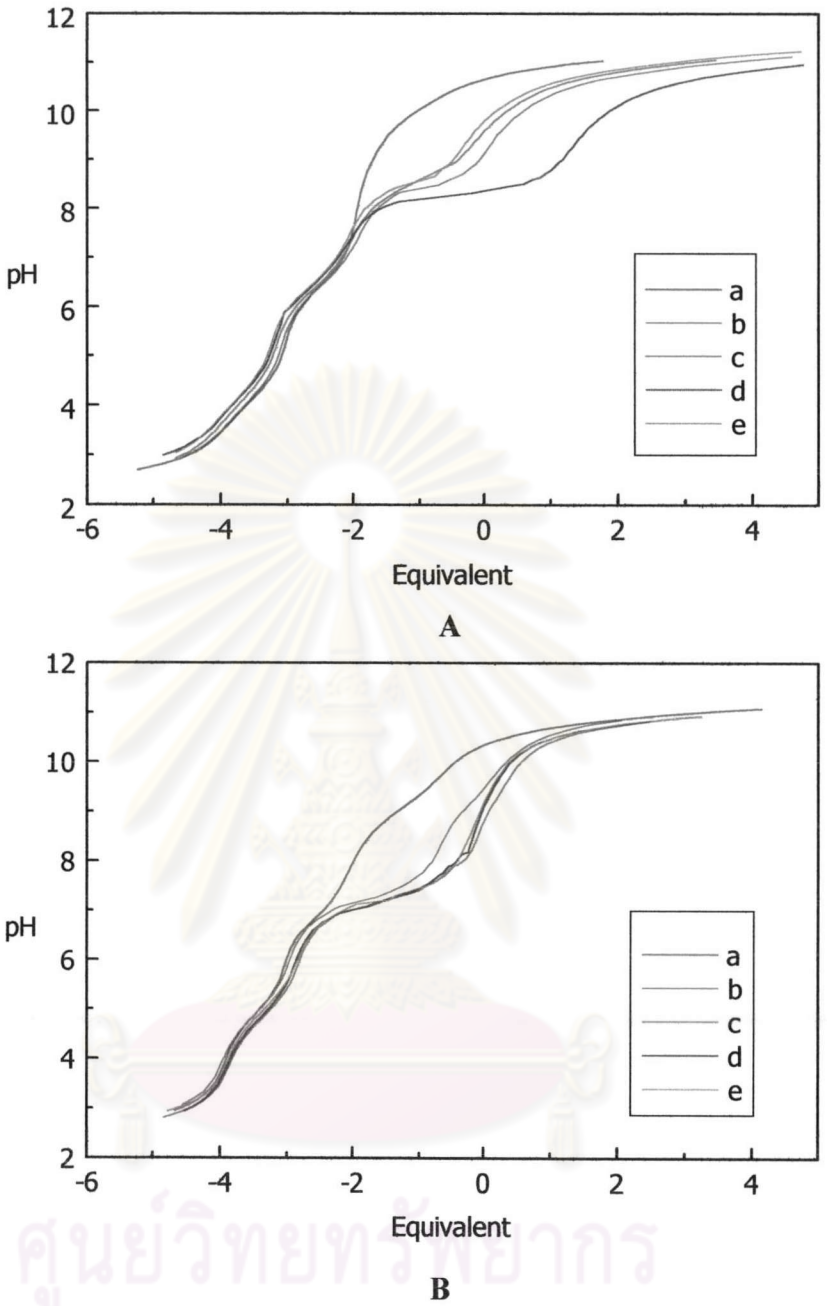

Figure 3.10 Potentiometric titration curves of

A) ligand **6a** with Co^{2+} ion at various ratio of **6a** : Co^{2+} : (a) 0.922 mM : 0 mM, (b) 0.876 mM : 0.871 mM, (c) 0.839 mM : 0.835 mM, (d) 0.839 mM : 0.835 mM and (e) 0.805 mM : 1.602 mM.

B) ligand **6b** with Co^{2+} ion at various ratio of **6b** : Co^{2+} : (a) 0.915 mM : 0 mM, (b) 0.873 mM : 0.883 mM, (c) 0.837 mM : 0.847 mM, (d) 0.873 mM : 0.869 mM and (e) 0.772 mM : 0.771 mM.

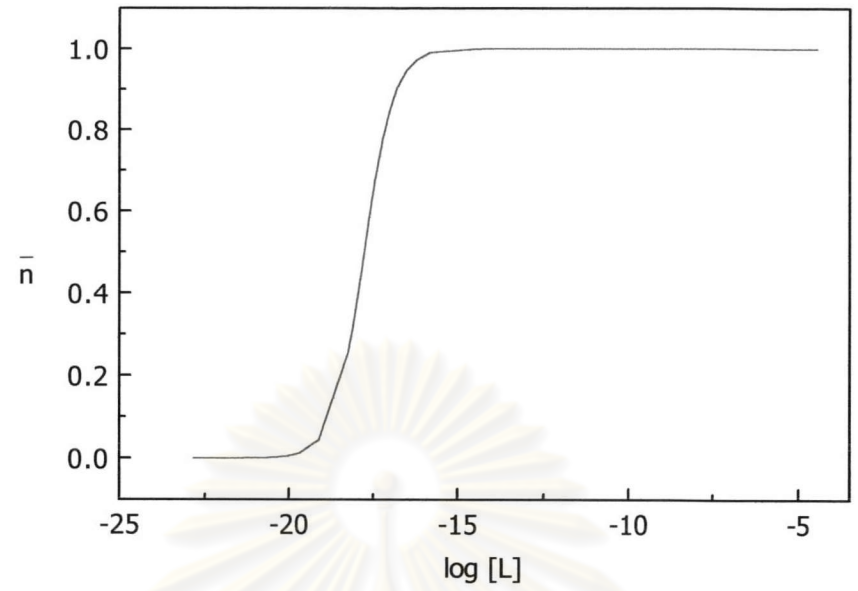

A

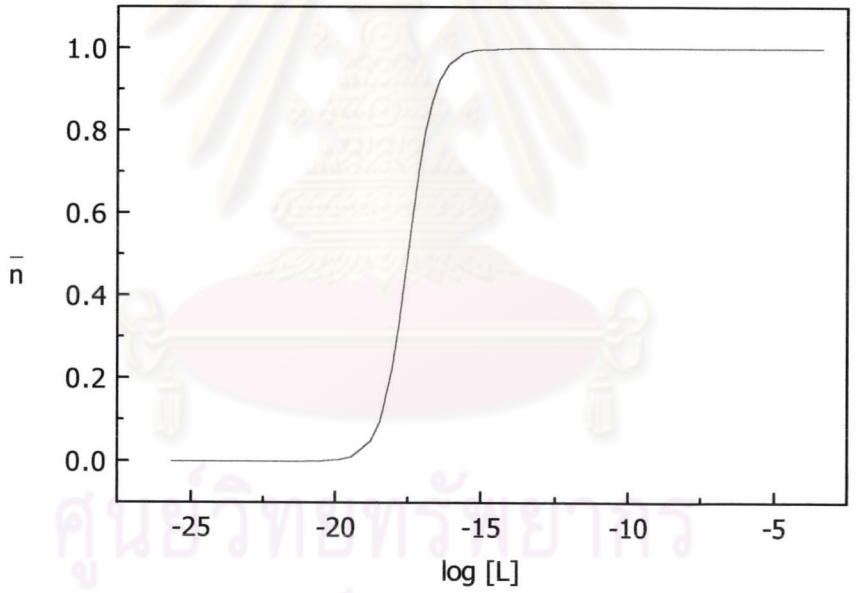

B

Figure 3.11 Plots between $\bar{n}$ versus the log [L] for Cu^{2+} complexes with **A)** ligand **6a** at the concentration ratio (**6a**:Cu^{2+}) of 0.811 mM : 1.625 mM and **B)** ligand **6b** at the concentration ratio (**6b**:Cu^{2+}) of 0.845 mM : 0.846 mM.

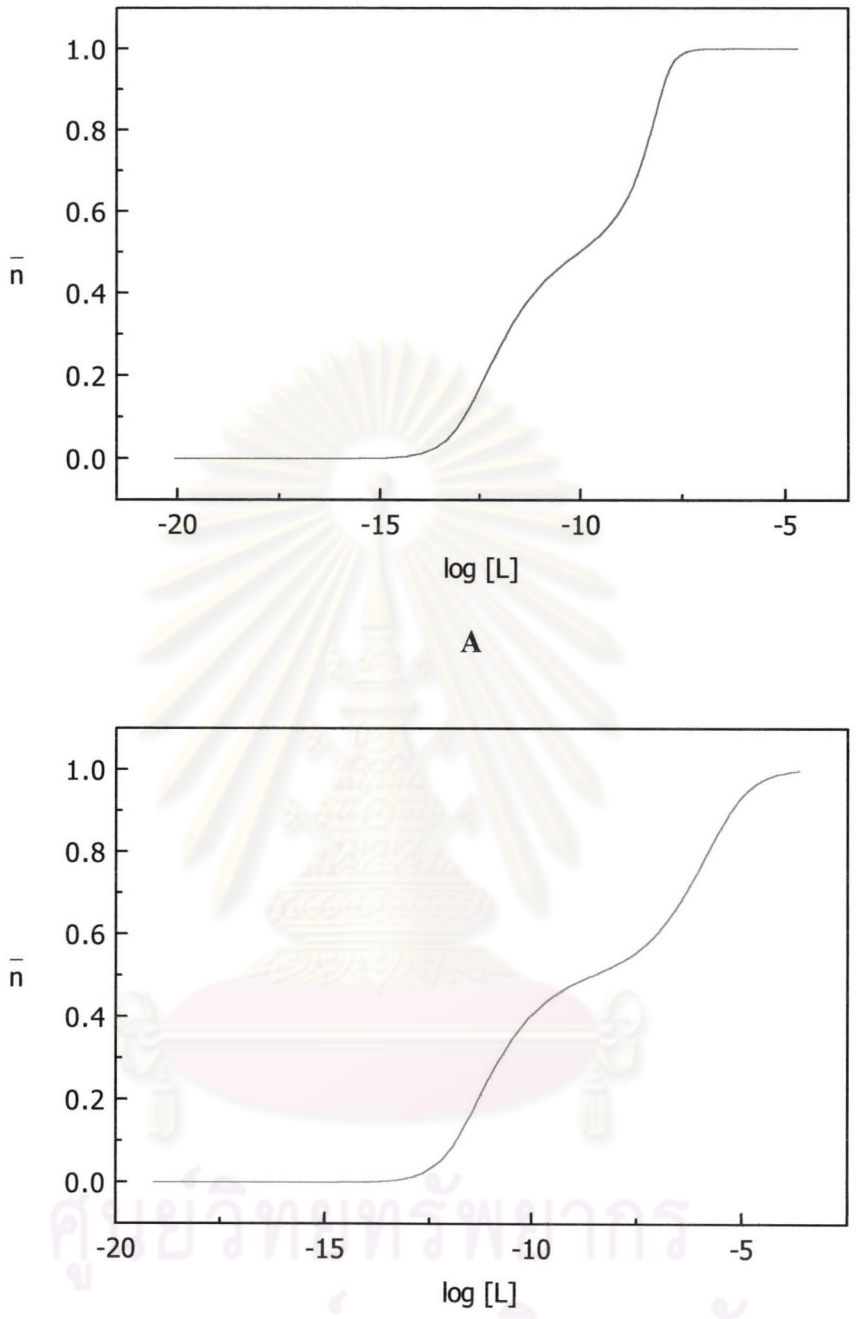

Figure 3.12 Plots between $\bar{n}$ versus the log [L] for Zn^{2+} complexes with **A**) ligand **6a** at the concentration ratio (**6a**:Zn^{2+}) of 0.805 mM : 1.629 mM and **B**) ligand **6b** at the concentration ratio (**6b**:Zn^{2+}) of 0.775 mM : 1.566 mM.

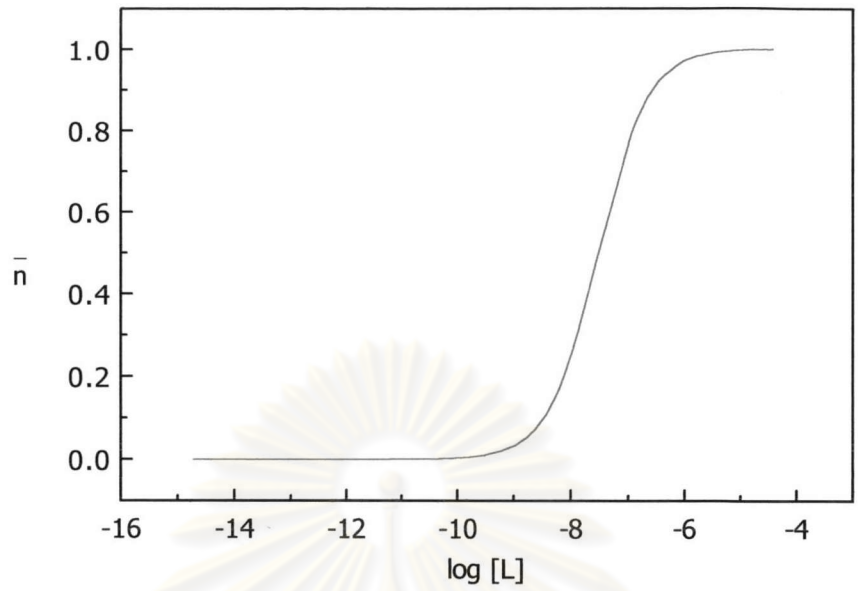

A

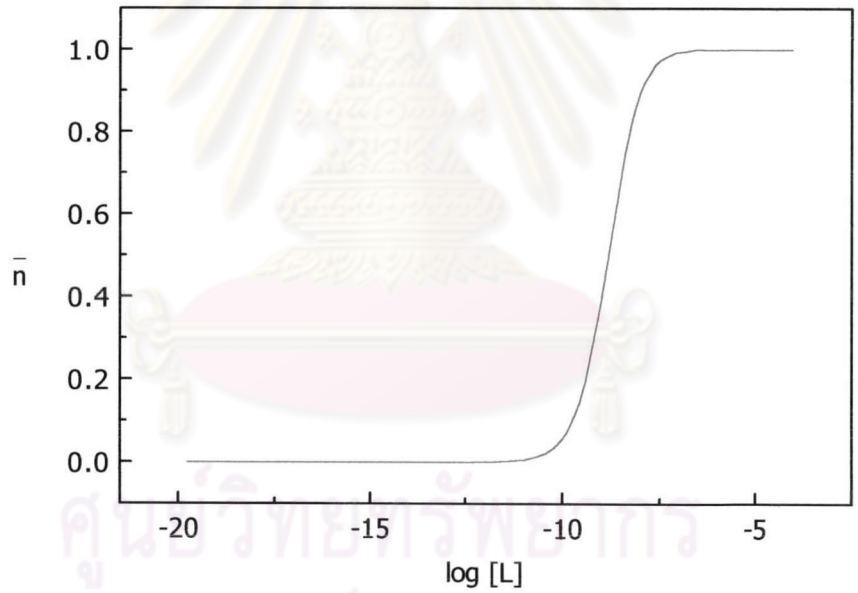

B

Figure 3.13 Plots between $\bar{n}$ versus the log [L] for Co^{2+} complexes with **A**) ligand **6a** at the concentration ratio (**6a**:Co^{2+}) of 0.839 mM : 0.835 mM and **B**) ligand **6b** at the concentration ratio (**6b**:Co^{2+}) of 0.837 mM : 0.847 mM.

Stability constants of metal complexes of calix[4]arene derivatives **6a** and **6b** expressed in terms of overall logarithmic values (log β) are summarized in Table 3.3.

Table 3.3 Stability constants of complexes of **6a** and **6b** towards Co^{2+}, Cu^{2+} and Zn^{2+} ions in 1.00 x 10^{-2} M $Bu_4NCF_3SO_3$ in methanol at 25 °C

Ligand	Species of complexes	log β		
		Co^{2+}	Cu^{2+}	Zn^{2+}
6a	ML^{2+}	7.52 ± 0.02	17.75 ± 0.06	9.97 ± 0.06
	M_2L^{4+}	-	-	15.31 ± 0.06
	$ML(OH)^+$	-	-	1.17 ± 0.07
6b	ML^{2+}	8.75 ± 0.04	17.50 ± 0.07	8.52 ± 0.07
	M_2L^{4+}	-	-	14.28 ± 0.05
	$ML(OH)^+$	0.42 ± 0.06	-	-

Furthermore, logarithms of the stepwise formation constants determined in 1.00 x 10^{-2} M $Bu_4NCF_3SO_3$ in methanol at 25 °C for the complexation reactions of **6a** and **6b** with Zn^{2+} and Co^{2+} are reported in Tabled 3.4 and 3.5, respectively.

Table 3.4 Stepwise formation constants of complexes of **6a** and **6b** towards Zn^{2+} in 1.00 x 10^{-2} M $Bu_4NCF_3SO_3$ in methanol at 25 °C

Equilibrium reaction	log K	
	6a	**6b**
$L + Zn^{2+} \rightleftharpoons ZnL^{2+}$	9.97 ± 0.06	8.52 ± 0.07
$ZnL^{2+} + Zn^{2+} \rightleftharpoons Zn_2L^{4+}$	5.34 ± 0.06	5.76 ± 0.05
$ZnL^{2+} + OH^- \rightleftharpoons ZnL(OH)^+$	-8.80 ± 0.06	-

Table 3.5 Stepwise formation constants of complexes of **6a** and **6b** towards Co^{2+} in 1.00 x 10^{-2} M $Bu_4NCF_3SO_3$ in methanol at 25 °C

Equilibrium reaction	log K	
	6a	**6b**
$L + Co^{2+} \rightleftharpoons CoL^{2+}$	7.52 ± 0.02	8.75 ± 0.04
$CoL^{2+} + OH^- \rightleftharpoons CoL(OH)^+$	-	-8.33 ± 0.02

3.2.2.1 Nature of the complexes between calix[4]arenes 6a and 6b with Cu^{2+}, Zn^{2+} and Co^{2+} ions

According to Figures 3.8, 3.9 and 3.10, the decrease of pH was obviously observed between the titration curves of the calix[4]arene **6a** and **6b** alone and in the presence of metal ions. These results confirmed the formation of the metal complexes. The number and position of the equivalent points were indicative of the number and stoichiometry of the complexes formed, although in some cases the consideration of additional species led to significant improvement of the fit during the calculation process. During the titration experiments for determination of stability constants, the color of the solutions containing Cu^{2+} were changed from very pale blue at acidic range to deep blue in the basic condition. In the presence of Co^{2+}, uncommonly, the solutions were turned from very pale yellow to yellow during the addition of base instead of dark blue or pink, which are normal color found in cobalt (II) complexes. The colorless solutions were afforded from the experiments concerned with Zn^{2+} ion.

Both ligands **6a** and **6b** usually form mononuclear complexes (ML^{2+}) with Cu^{2+}, Zn^{2+} and Co^{2+} ions. Meanwhile, the differences between these two analogous compounds can also be observed. Calix[4]arene **6a** forms zinc complexes with ligand to metal cation ratio 1:1 and 1:2 (M_2L^{4+}) as same as found in ligand **6b**.

However, mononuclear zinc complex of **6a** is able to coordinate hydroxide ion leading to the formation of metal hydroxo complex ($ML(OH)^+$) while this species for **6b** is not observed even at the high pH value. On the other hand, mononuclear cobalt complex of **6a** shows no tendency to form hydroxo species in the solution while cobalt complex of ligand **6b** is capable. Partially protonated species such as MHL^{3+} or MH_2L^{4+} or MH_3L^{5+} are certainly not encountered in any experiment indicating that all four nitrogen atoms of the **tren** moiety in **6a** and **6b** were totally involved in metal coordination.

Similar to a plot between $\bar{n}$ and log [L], a species distribution diagram is also served as a good source of individual characteristic behaviour for each complex. The species distribution diagrams of the complexes of **6a** and **6b** with Cu^{2+}, Zn^{2+} and Co^{2+} are illustrated in Figures 3.14, 3.15 and 3.16, respectively

Copper(II) complexes of calix[4]arenes **6a** and **6b** are observed in metal to ligand ratio of 1:1 only. Dinuclear complexes or partially protonated species are not involved with coordination of Cu^{2+} ion. Ligands **6a** and **6b** are able to form copper(II) complexes even in the acidic range. The ratio of free Cu^{2+} ion and CuL^{2+} is 50:50 at pH = 4.7 and 4.6 for **6a** and **6b**, respectively (see Figure 3.14). The concentrations of mononuclear complex CuL^{2+} reach the highest value (100%) at pH = 5.80 (for **6a**) and 5.50 (for **6b**). After that, even in an alkaline solution, no hydroxo species are detected. This result indicates that the CuL^{2+} complexes of both calix[4]arenes are very stable and hard to be converted to the monovalent complexes.

Possible species when ligand **6a** forms complex with Zn^{2+} are ZnL^{2+}, Zn_2L^{4+} and $ZnL(OH)^+$. The binuclear complex is the predominant species at the pH range of 7.2 to 8.6 with the highest population is 43%. The amount of the mononuclear complex is not higher than 28% and this species exists at the pH range of 8 to 10. In basic solution, the $ZnL(OH)^+$ is the predominant complex and its amount is increased as a function of pH with the highest population of 98% at pH = 10.4. In case of ligand **6b**, the binuclear complex appears in the middle of the pH range (with highest amount of 46%) and ZnL^{2+} is formed at pH above 8.0 and over 80% of its population appear at pH above 9.3 (Figure 3.15).

CoL^{2+} is the major product from the formation reaction between **6a** and Co^{2+}. This mononuclear complex is formed at pH over 9 with at least 50% of its amount. However, for ligand **6b**, CoL^{2+} can undergoes the hydrolysis reaction and afford metal hydroxo $CoL(OH)^{+}$ as a predominant species at pH above 8.4 and its exists 70% at minimum pH value of 8.7. The mononuclear complex of **6b** with Co^{2+} appears at the pH range of 6.9 to 9.8 and its highest amount is about 60% at pH = 7.94 (see Figure 3.16).

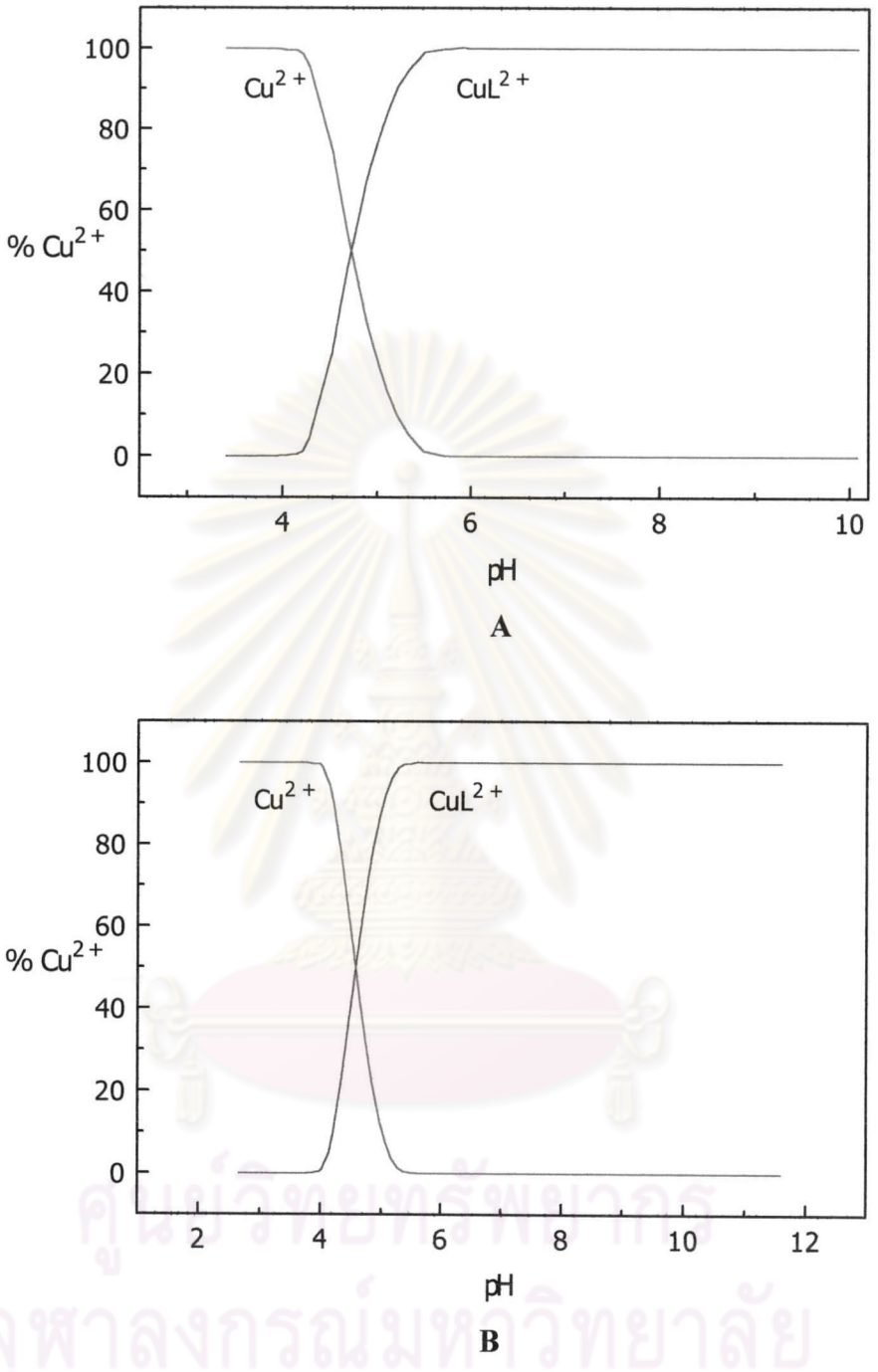

Figure 3.14 Species distribution diagrams of the Cu^{2+} complexes in 1.00 x 10^{-2} M $Bu_4NCF_3SO_3$ in methanol at 25°C with **A**) ligand **6a** at the concentration ratio (**6a**:Cu^{2+}) of 0.811 mM : 1.625 mM and **B**) ligand **6b** at the concentration ratio (**6b**:Cu^{2+}) of 0.845 mM : 0.846 mM.

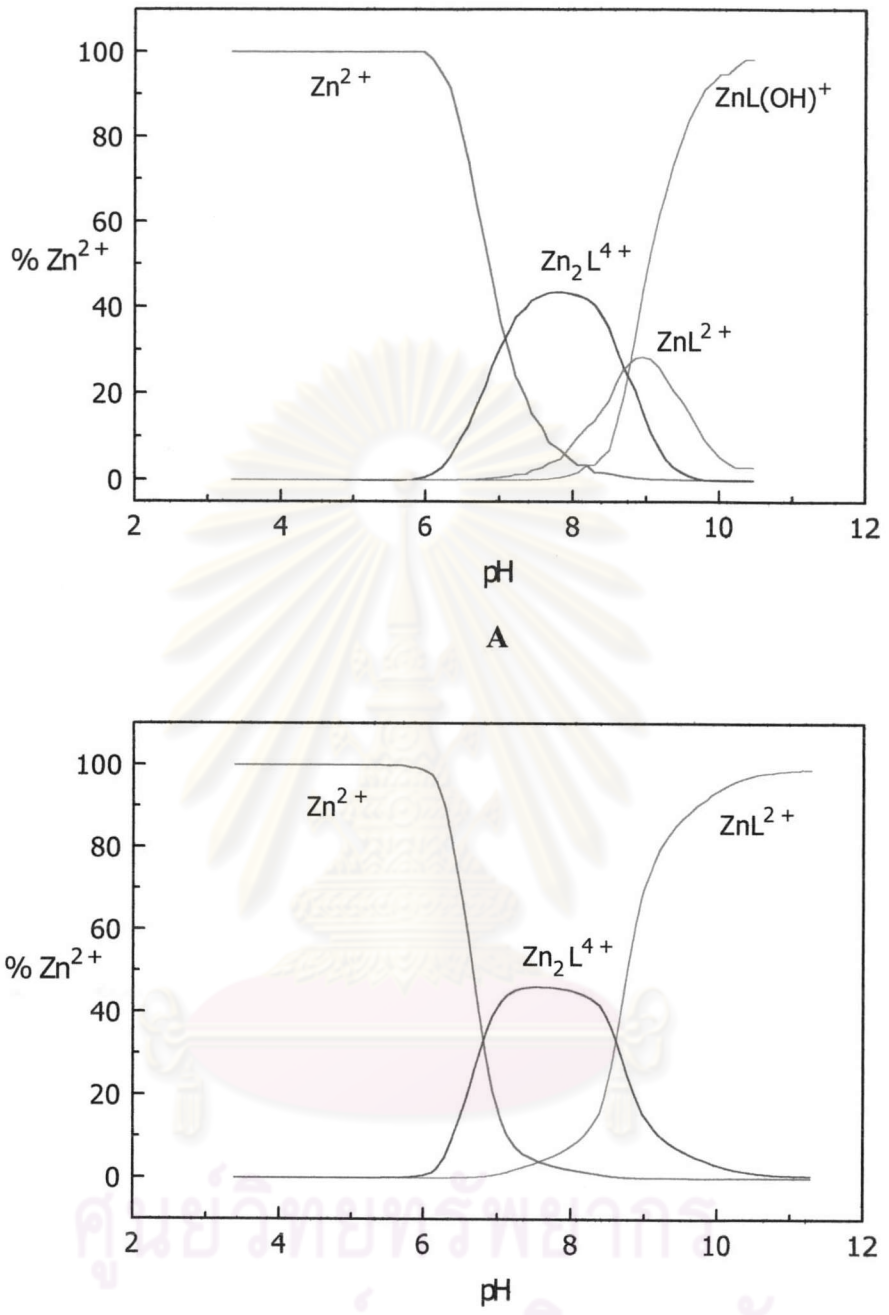

Figure 3.15 Species distribution diagrams of the Zn^{2+} complexes in 1.00 x 10^{-2} M $Bu_4NCF_3SO_3$ in methanol at 25°C with **A)** ligand **6a** at the concentration ratio (**6a**:Zn^{2+}) of 0.805 mM : 1.629 mM and **B)** ligand **6b** at the concentration ratio (**6b**:Zn^{2+}) of 0.775 mM : 1.566 mM.

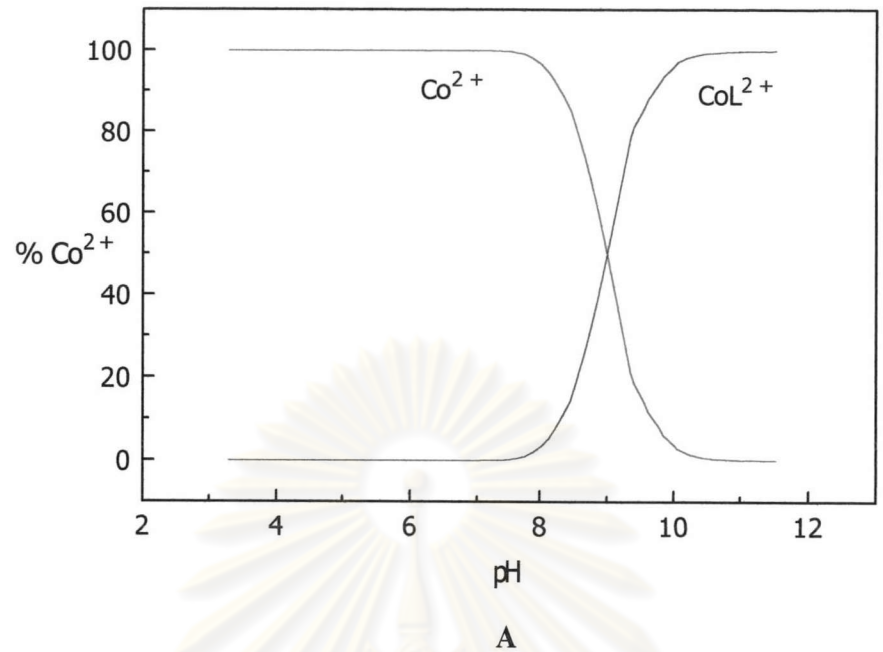

A

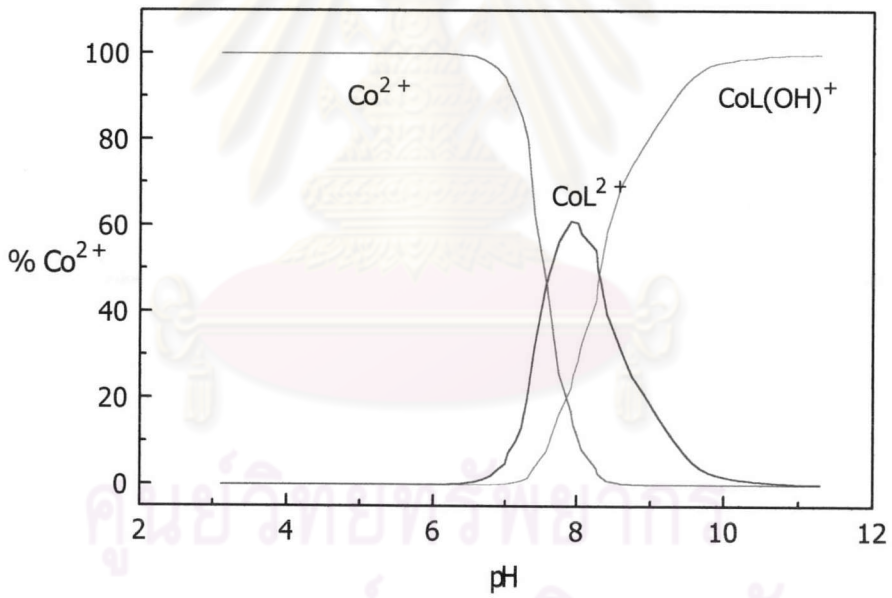

B

Figure 3.16 Species distribution diagrams of the Co^{2+} complexes in 1.00 x 10^{-2} M $Bu_4NCF_3SO_3$ in methanol at 25°C with **A**) ligand **6a** at the concentration ratio (**6a**:Co^{2+}) of 0.839 mM : 0.835 mM and **B**) ligand **6b** at the concentration ratio (**6b**:Co^{2+}) of 0.837 mM : 0.847 mM.

From the results described in section 3.2.2.1, they imply that three transition metal ions, Cu^{2+}, Co^{2+} and Zn^{2+}, are able to include into the cavity of host molecules **6a** and **6b**. Both secondary and tertiary amine groups of the **tren** moiety are involved in the coordination character of these two ligands. Copper(II) and cobalt(II) complexes of **6a** and **6b** possess metal to ligand ratio of 1:1 or can be mentioned that only mononuclear species are formed. Therefore, both metal ions are very likely bound at the cavity of the **tren** unit. Compounds **6a** and **6b** also exhibit the high tendency to form binuclear complex during the formation reactions with Zn^{2+}. This result may lead to the suggestion that another zinc ion is allowed to accommodate in ligands **6a** and **6b** at the glycolic chain unit, which located near the phenolic oxygen of calix[4]arene, besides the other cation that bound among nitrogen donor atoms. This concept is reasonable because zinc ion is oxophilic and shows tendency to form stable complex with hosts which containing oxygen donors. In 1997, Tuntulani and his coworkers reported the preliminary complexation studies of ligand **6a** with zinc ion by means of ^{1}H-NMR spectroscopy.[89] In the presence of 1:1 metal to ligand ratio, the ethylene protons of the **tren** unit were shifted downfield from 2.66 to 2.75 ppm indicating that zinc ion has an interaction with nitrogen donors. Nevertheless, when the second equivalent of Zn^{2+} was added, the ^{1}H-NMR spectrum showed another migration of glycolic chain protons from 4.32 to 4.44 ppm in addition to the significant shift of that in NHC$\mathbf{H}_2$C$\mathbf{H}_2$NH part. This implies that the zinc ion probably resides in the crown unit near the lower rim of calix[4]arene. Hence, from all results that previously described lead us to propose the structure of transition metal complexes of ligand **6a** and **6b** as shown in Figure 3.15.

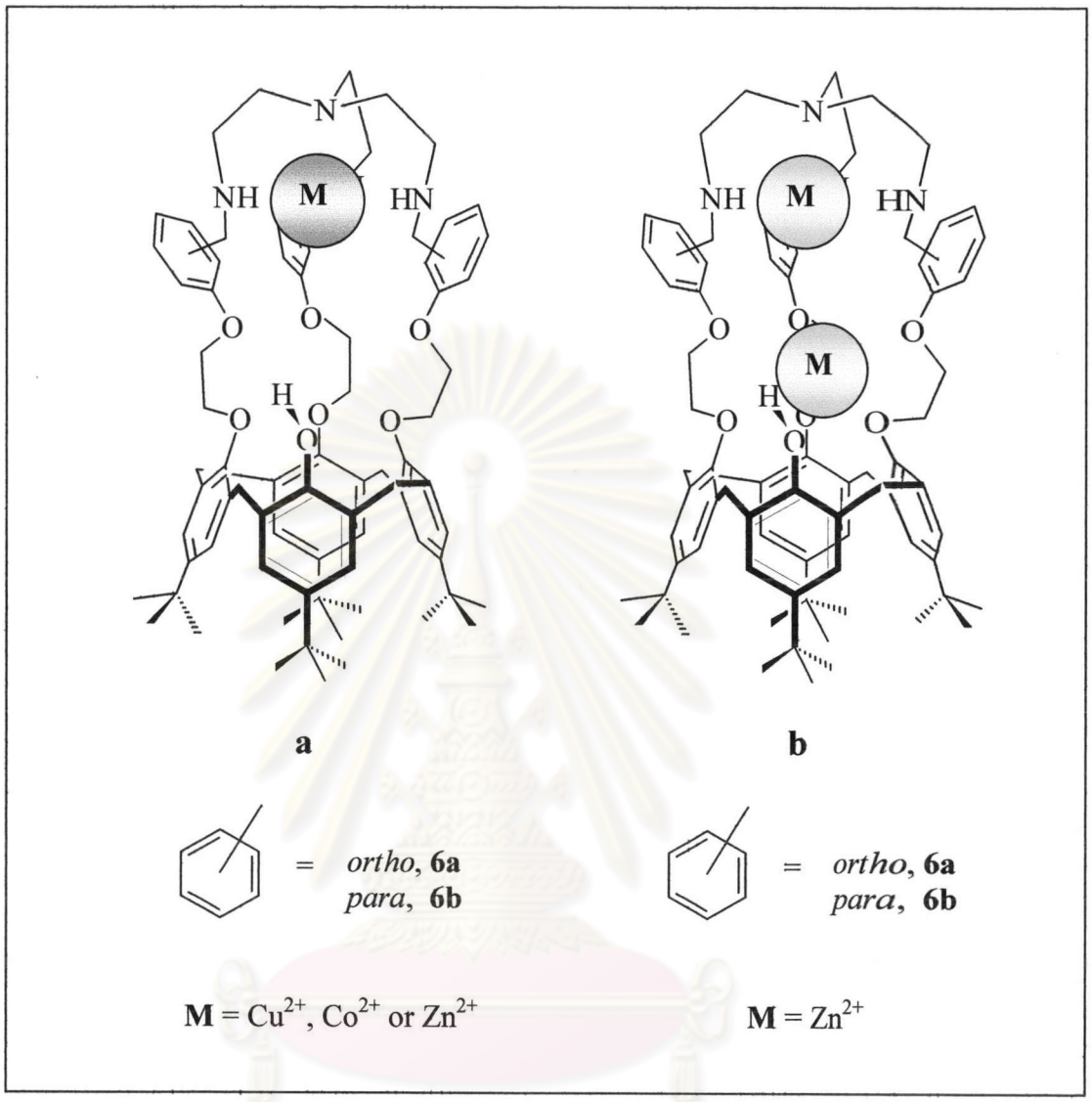

Figure 3.17 Proposed structures of complexes of **6a** and **6b** with Co^{2+}, Cu^{2+} and Zn^{2+} **a**) 1:1 complexes and **b**) 1:2 complexes.

3.2.2.2 Stability of the Complexes of Calix[4]arenes 6a and 6b with Cu^{2+}, Zn^{2+} and Co^{2+} ions

According to the logarithm of overall stability constants that reported in Table 3.3, the copper complexes of both **6a** and **6b** are very stable, as shown by the high values of log β for 1:1 complex. Ligand **6a** shows slightly higher stability constants than **6b** with the difference of 0.25 log units. This result suggests that the size of binding unit in **6a** is smaller than **6b** because of the effect of *ortho* substituents. Hence, Cu^{2+} ion can be firmly bound with nitrogen donors in **6a** more than that in **6b** and leading to the high stability constant. However, this difference is non-significant and we can conclude that the binding abilities of **6a** and **6b** towards Cu^{2+} are quite similar. In addition, when Cu^{2+} is accommodated in the **tren** moiety, the nitrogen atoms will arrange themselves in order to obtain the appropriate position for the strongest interaction. This action may lead the trigonal bypiramidal geometry, which is the most common geometry found in many copper(II) complexes. Another ligand that will occupy at the axial position of metal center is a solvent molecule such as water or methanol in the presence of non-coordinating counteranions (such as ClO_4^- or $CF_3SO_3^-$). This assumption are supported by the X-ray crystal structures of various copper(II) complex of symmetric and unsymmetric tripodal tetramine ligands which their structures are similar to the **tren** unit .[90]

When the cation is changed to Zn^{2+}, as similar to their Cu^{2+} complex analogues, ligand **6a** forms both mononuclear and binuclear complexes more stable than **6b**. These data can be interpreted by considering the size of the binding moiety in **6a** and **6b**. Ligand **6b** possesses a more flexible structure and each donor atom is separated apart more than those in **6a**. Because of the smaller ionic radius of Zn^{2+} in comparison with Cu^{2+}, the smaller binding site in **6a** is more appropiate than the larger cavity in ligand **6b**. These results are encouraged by the difference of overall stability constants between zinc complexes of **6a** and **6b** (1.45 and 1.03 in logarithmic unit for mononuclear and binuclear complexes, respectively).

However, if we consider the stepwise formation constant, it is quite surprising that the binding affinity of the second zinc ion for the 1:1 complex of **6b** is slightly higher than **6a** (see Table 3.4). This result can also be rationalized in a term of the more cavity of the host molecule. Distance between the **tren** unit and glycolic ether chains in **6b** is longer than that in **6a**. Therefore, when another zinc ion is included in to the position nearby the lower rim of calix[4]arene, the total electronic repulsion is decreased and lead to greater chance to form a binuclear complex in case of **6b**. Ligand **6a** also undergoes hydrolysis reaction and affords $ZnL(OH)^+$, which is largely prevalent in an alkaline solution. The logarithm of overall stability constant and stepwise formation constant for this species are 1.17 and –8.80, respectively.

In contrast to Zn^{2+} ion, the complexes of cobalt(II) ion and ligands **6a** and **6b** are totally existed in 1:1 metal to ligand ratio. When consider the log β values of Co^{2+} complexes of **6a** and **6b**, it is obvious that the tendency of the stability constant is **6b > 6a** (the difference is about 1.25 logarithm units). This phenomenon is also able to explain in the same manner as zinc complexes. Co^{2+} ion is larger than Cu^{2+} and Zn^{2+} and requires more space to form a complex. The cavity of binding site in calix[4]arene **6b** is quite matched with cobalt(II) ionic radius and lead to a more stable complex than **6a**. Furthermore, the geometry of the metal center is probably trigonal bipyramidal (tbp) similar to copper and zinc complexes, and only **6b** is capable to the addition of hydroxide ion to the corresponding mononuclear complexes. The overall and stepwise formation constants of $CoL(OH)^+$ species is 0.42 and -8.83, respectively.

Due to the data that reported in Table 3.3, we can summarized the order of the stability constants for mononuclear complexes of ligands **6a** and **6b** with three cations as follows:

$$Co^{2+} << Cu^{2+} >> Zn^{2+}$$

This order is correspond with the Irving-Williams sequence, which always employed as reference series for the order of stability constants.[91] Unfortunately, the stability constants of Ni^{2+} complexes are not obtained from this experiment due to their slow solvent exchange reactions leading to the long time required for the equilibrium

reactions.[92] The rate constant for solvent exchange reaction of Ni^{2+} ion in methanol is about 10^4 and 10 times lower than Cu^{2+} and Co^{2+} ions, respectively (See Table 3.6). This implies that the reaction containing Ni^{2+} ions requires more times to reach the equilibrium. Therefore, the magnitude of stability constants for Ni^{2+} complexes of both **6a** and **6b** are expected to lower than other cations. This assumption is quite reasonable when consider other results that obtained from complexation studies of related host molecules such as *tris*[2-(dimethylamino)ethyl]amine (Me_6**tren**). RGT, R3Bm and R3Bp (see Figure 3.5). The stability constants of these cryptands and tripodal amine with Co^{2+}, Ni^{2+}, Cu^{2+} and Zn^{2+} are summarized in Table 3.7.

Table 3.6 Kinetic parameters for metahanol exchange of first-row divalent transition metal ions, $M(CH_3OH)_6^{2+}$ at 25 °C.[93]

	Mn^{2+}	Fe^{2+}	Co^{2+}	Ni^{2+}	Cu^{2+}
k, s^{-1}	3.7×10^5	5.0×10^4	1.8×10^4	1.0×10^3	3.1×10^7
$\Delta H^{\ddagger}$, kJ mol^{-1}	26	50	58	66	17
$\Delta S^{\ddagger}$, J K^{-1} mol^{-1}	-50	+13	+30	+34	-44
$\Delta V^{\ddagger}$, cm^3 mol^{-1}	-5.0	+0.4	+8.9	+11.4	+8.3

Table 3.7 Logarithm of stability constants of complexes of compounds $Me_6$the **tren**, RGT, R3Bm and R3Bp with transition metal cations at 25°C. (Shown only the stability constants of important species such as ML^{2+}, M_2L^{4+} $MLOH^+$ or partially protonated species)

Ligand	Complex	Ni^{2+}	Co^{2+}	Cu^{2+}	Zn^{2+}
Me_6**tren** [A]	ML^{2+}	**7.14 ± 0.04**	**8.53 ± 0.03**	**15.65 ± 0.03**	**9.75 ± 0.04**
	M_2L^{4+}	-	-	-	-
R3Bm [B]	ML^{2+}	**5.50 ± 0.06**	**7.53 ± 0.03**	-	-
	M_2L^{4+}	-	-	**25.86 ± 0.05**	-
	$MLOH^+$	-4.6 ± 0.1	-	-	-
	MLH^{3+}	-	16.41 ± 0.03	-	-
R3Bp [B]	ML^{2+}	**4.3 ± 0.2**	**6.9 ± 0.4**	nd [C]	-
	MLH^{3+}	12.7 ± 0.1	15.8 ± 0.2	nd [C]	-
RGT [B]	MLH^{2+}	15.16 ± 0.05	-	-	18.87 ± 0.07
	MLH_2^{4+}	-	-	-	25.11 ± 0.01
	MLH_3^{5+}	-	30.3 ± 0.2	33.38 ± 0.01	-

Note: A) studied in 1.0 M $NaClO_4$ solution (aqueous system).[94]

B) studied in 0.1 M Et_4NClO_4 solution (aqueous system).[86]

C) not determined.

According to the results that shown in Table 3.6, it is clear that all nickel(II) complexes of related compounds of **6a** and **6b** such as R3Bm and R3Bp exhibit the lowest stability constants compared to the other metal complexes. The sequence of each ligand is different from the Irving-Williams series. The major reason for this unusually result can be interpreted in term of the geometry of the complexes. Common coordination number for Ni^{2+} complex is 4, which regards to possible two geometries: tetrahedral and square planar. Although all ligands that derived from the **tren** molecule posses 4 nitrogen atoms, all donor positions are not available to adopt

such geometries because of the rigidity of the **tren** unit. This reason leads to the significant lower stability constants of nickel mononuclear complex of this type of ligand. The only 1:1 complexation of Me_6tren towards Zn^{2+} ion indicates that the presence of the calix[4]arene unit in **6a** and **6b** allows the formation of the 1:2 species. However, the real difference of ligands **6a** and **6b** in comparison with R3Bm and R3Bp is both octaaminocryptands form no 1:1 complex when the metal ions are Cu^{2+} and Zn^{2+} but formation of mononuclear complexes is possibly occurred in the presence of cobalt and nickel ions.

The other effect that controls the stability constants for complexes of **6a** and **6b** with first-row transition metal ions is 'The Cryptate Effect'. Cu^{2+} complexes of **6a** and **6b** are more stable than the 1,3-disubstitued calix[4]arene containing three nitrogen atoms, which was studied its binding ability towards first row transition metal ions by Suwattanamala and his colleagues.[95] The complexation properties of that triaza calix[4]arene was carried out by means of potentiometric titration. The inert background solution was 5.00 x 10^{-2} M $Bu_4NCF_3SO_3$ in methanol and all titration were performed at 25 °C. The stability constants of that calix[4]arene for Cu^{2+} complex was 15.27, about 100 times lower than the values from copper complexes of ligands **6a** and **6b**. This data can be rationalized that ligands **6a** and **6b** are cage molecules with greater rigidity of the structures than triaza calix[4]arene which is only a macrocyclic compound possesses two-dimensional structure. When a metal complex is formed, ligands **6a** and **6b** can strongly bind a cation with less interference of solvent molecules and counteranions. The formation reaction releases many free particles such as solvent molecules to the system leading to the high entropy (ΔS) change as well as an enthalpy (ΔH) variation. This results in the enormous alteration of Gibb's free energy of overall reaction (ΔG) which exhibited in the term of high stability constants of complexes.

3.2.2.3 Complexation selectivities of Calix[4]arenes 6a and 6b towards Cu^{2+}, Zn^{2+} and Co^{2+} ions

The selectivity for one cation (M^1) relative to another (M^2) can be expressed as the ratio of the stability constants as follows:

$$S_1(M^1/M^2) = \beta_{110}(M^1)/\beta_{110}(M^2) \quad \text{or} \quad S_2(M^1/M^2) = \beta_{210}(M^1)/\beta_{210}(M^2)$$

when β_{110} and β_{210} are noted as the overall stability constant of a mononuclear and a binuclear complex, respectively.[96,97] All selectivities for ligands **6a** and **6b** in the presence of metal cations are shown in Table 3.8.

Table 3.8 Selectivities of complexation for calix[4]arene derivatives **6a** and **6b** with Co^{2+}, Cu^{2+} and Zn^{2+}: $S_1(M^1/M^2) = \beta_{110}(M^1)/\beta_{110}(M^2)$.

Selectivities ($S_1(M^1/M^2)$)	Calix[4]arene	
	6a	**6b**
$S_1(Cu^{2+}/Zn^{2+})$	6.02×10^7	9.55×10^8
$S_1(Cu^{2+}/Co^{2+})$	1.70×10^{10}	5.62×10^8
$S_1(Zn^{2+}/Co^{2+})$	281.8	0.5888

As illustrated in Table 3.8, both ligands **6a** and **6b** show a high selectivity for Cu^{2+} over Zn^{2+} and Cu^{2+} over Co^{2+}. The selectivity for Cu^{2+} over Zn^{2+} in presence of **6a** is about 10^7 while this value for **6b** is 10^8. This result indicates the more selectivity of ligand **6b** towards Cu^{2+} over Zn^{2+} in the mixed metal solution. However, when compare between Cu^{2+} and Co^{2+}, ligand **6a** shows higher selectivity towards Cu^{2+} over Co^{2+} than **6b** ($S_1 \approx 10^{10}$ for **6a** and $S_1 \approx 10^8$ for **6b**). In addition, when consider the system of mixed Co^{2+} and Zn^{2+}, ligand **6a** expresses the greater tendency of selectivity for Zn^{2+} over Co^{2+}. On the other hand, ligand **6b** shows no significant difference of selectivity between these two cations ($S_1 = 0.58$) due to the almost equal stability constants of the zinc and cobalt mononuclear complexes.